EARTHQUAKE ENGINEERING AND STRUCTURAL DYNAMICS
Earthquake Engng Struct. Dyn. 2000; **29**:85–107

Effect of viscous, viscoplastic and friction damping on the response of seismic isolated structures

Nicos Makris*,† and Shih-Po Chang‡

Department of Civil and Environmental Engineering, SEMM, University of California at Berkeley, MC 1710, Berkeley, CA 94720, U.S.A.

SUMMARY

In this paper the efficiency of various dissipative mechanisms to protect structures from pulse-type and near-source ground motions is examined. Physically realizable cycloidal pulses are introduced, and their resemblance to recorded near-source ground motions is illustrated. The study uncovers the coherent component of some near-source acceleration records, and the shaking potential of these records is examined. It is found that the response of structures with relatively low isolation periods is substantially affected by the high-frequency fluctuations that override the long duration pulse. Therefore, the concept of seismic isolation is beneficial even for motions that contain a long duration pulse which generates most of the unusually large recorded displacements and velocities. Dissipation forces of the plastic (friction) type are very efficient in reducing displacement demands although occasionally they are responsible for substantial permanent displacements. It is found that the benefits by hysteretic dissipation are nearly indifferent to the level of the yield displacement of the hysteretic mechanism and that they depend primarily on the level of the plastic (friction) force. The study concludes that a combination of relatively low friction and viscous forces is attractive since base displacements are substantially reduced without appreciably increasing base shears and superstructure accelerations. Copyright © 2000 John Wiley & Sons, Ltd.

KEY WORDS: near-source ground motions; seismic isolated structures; viscous damping, hysteretic damping

INTRODUCTION

The dynamic response of a structure depends on its mechanical characteristics and the nature of the induced excitation. Mechanical properties which are efficient to mitigate the structure's

*Correspondence to: Nicos Makris, Department of Civil and Environmental Engineering, Structural Engineering Mechanics and Materials (SEMM), University of California at Berkeley, 721 Davis Hall, Berkeley, CA 94720-1710, U.S.A.
†Associate Professor.
‡Graduate Research Assistant.

Contract/grant sponsor: National Science Foundation; contract/grant number: CMS-9696241.
Contract/grant sponsor: California Department of Transportation; contract/grant number: RTA-59A169.

Received 17 December 1998
CCC 0098–8847/2000/010085–23$17.50 *Revised 20 August 1999*

Accepted 24 August 1999

response when subjected to certain inputs might have an undesirable effect during other inputs. Ground motions generated from earthquakes differ from one another in magnitude, source, characteristics, distance and direction from the rupture location and local soil conditions. The ability of a structure to dissipate energy is central to controlling displacement demands, and various energy dissipation mechanisms have been proposed to enhance structural response [1]. These energy dissipation mechanisms can be of various types such as viscous, rigid–plastic, elastoplastic, viscoplastic, or combination of thereof.

Under seismic excitations that have relatively long durations, a structure undergoes several cycles during the forced vibration part of the response; therefore, its response depends more on the amount of energy that is dissipated during each cycle (area under the force–displacement loop) than on the nature of the dissipative force that develops (viscous, friction, elastoplastic or viscoplastic). Because of this, the dissipation properties of structures are averaged over a cycle of motion and are expressed in terms of dimensionless ratios which originate from the linear theory of structural dynamics. Within the context of linear viscoelasticity the effect of linear damping on the response of isolated structures subjected to stationary random excitations was addressed in depth by Inaudi and Kelley [2].

During the last two decades, an ever increasing database of recorded ground motions have demonstrated that the kinematic characteristics of the ground motion near the faults of major earthquakes contain large displacement pulses from 0.5 m more than 1.5 m with peak velocities of 0.5 m/sec or higher. In some cases, the coherent pulse is distinguishable not only in the displacement and velocity histories, but also in the acceleration history, which happens to be a rather smooth signal. In other cases, acceleration histories recorded near the source contain high-frequency spikes and resemble the traditional random-like signal; however, their velocity and displacement histories uncover a coherent long-period pulse with some overriding high-frequency fluctuations [3–5].

The challenge in providing seismic protection from such motions is the selection of mechanical properties that will improve the response of a structure subjected to a high-frequency spike and a low-frequency, low-acceleration pulse. Previous studies [6–8] indicated that what makes near-source ground motions particularly destructive to some structures is not their peak ground acceleration but the 'incremental' ground velocity which is the net increment of the ground velocity along a monotonic segment of its time history. These indications challenged the concept of seismic isolation. This paper addresses this challenge in a systematic way, showing that seismic isolation is effective against near-source ground motions provided that the appropriate energy dissipation mechanism is provided.

In this study the effect of various dissipation mechanisms in reducing the response of seismically isolated structures subjected to near-source ground motions is examined in detail. Selected near-source ground motions are presented, and their resemblance to physically realizable cycloidal pulses is shown. A type-A cycloidal pulse approximates a forward motion; a type-B cycloid pulse approximates a forward-and-back motion; whereas, a type-C_n pulse approximates a recorded motion that exhibits n main pulses in its displacement history. The velocity histories of all type-A, type-B and type-C_n pulses are differentiable signals that result in finite acceleration values.

While the proposed cycloidal pulses capture many of the kinematic characteristics of the displacement and velocity histories of recorded near-source ground motions, in many cases the resulting accelerations are poor predictions of the recorded histories. This is because in many near-source ground motions there are high-frequency fluctuations that override the

long-duration pulse. It is shown that the response of structures with relatively low isolation periods is affected significantly by these high-frequency fluctuations, indicating that the concept of seismic protection by lengthening the isolation period is beneficial when the approximate type of energy dissipation is provided. The benefits of rigid–plastic or elastic–plastic behaviour are nearly indifferent to the level of the yield displacement and depend primarily on the level of the plastic (friction) force. The paper concludes that a combination of relatively low values of plastic (friction) and viscous damping results in an attractive design since displacements are substantially reduced without increasing appreciably base shears and superstructure accelerations.

CLOSED-FORM APPROXIMATION OF NEAR-SOURCE GROUND MOTIONS

Figure 1 (left) shows the fault normal components of the acceleration, velocity and displacement histories of the 18 June 1992 Landers earthquake recorded at the Lucerne Valley station [5]. The motion resulted in a forward displacement of the order of 1.8 m. The coherent long-duration pulse responsible for most of this displacement can also be distinguished in the velocity history, whereas the acceleration history is crowded with high-frequency spikes. Figure 1 (right) plots the acceleration, velocity and displacement histories of a type-A cycloidal pulse given by the

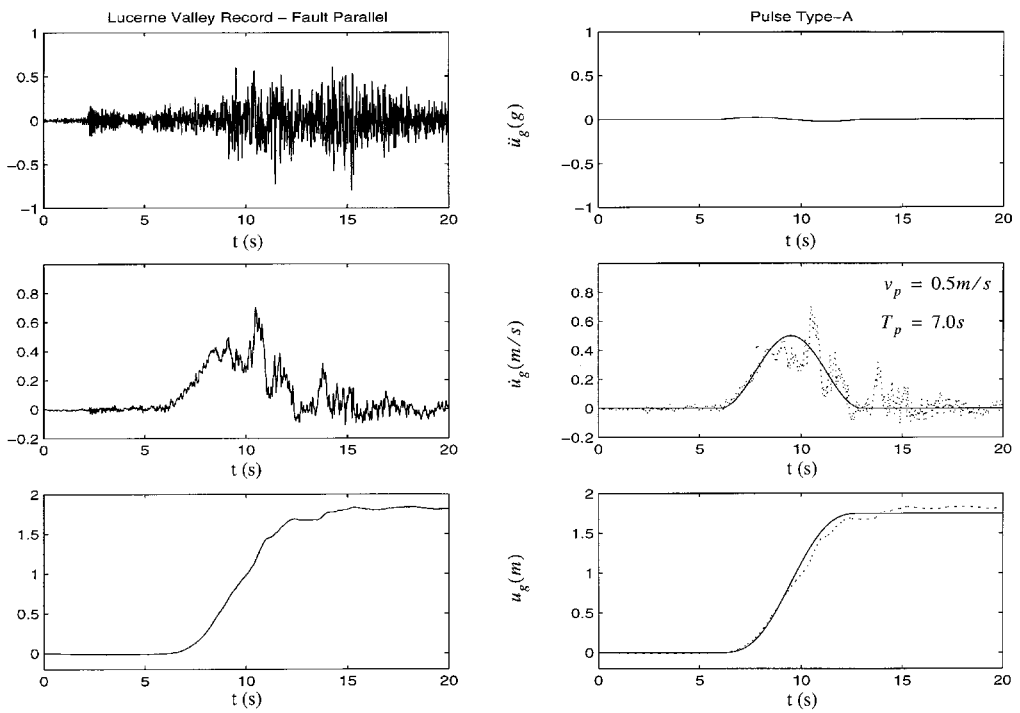

Figure 1. Fault parallel components of the acceleration, velocity and displacement time histories recorded at the Lucerne Valley station during the 28 June 1992 Landers, California earthquake (left), and a cycloidal type-A pulse (right).

following [9, 10]:

$$\ddot{u}_g(t) = \omega_p \frac{v_p}{2} \sin(\omega_p t), \quad 0 \leqslant t \leqslant T_p \tag{1}$$

$$\dot{u}_g(t) = \frac{v_p}{2} - \frac{v_p}{2} \cos(\omega_p t), \quad 0 \leqslant t \leqslant T_p \tag{2}$$

$$u_g(t) = \frac{v_p}{2} t - \frac{v_p}{2\omega_p} \sin(\omega_p t), \quad 0 \leqslant t \leqslant T_p \tag{3}$$

In constructing Figure 1 (right), the values of $T_p = 7.0\,\text{s}$ and $v_p = 0.5\,\text{m/s}$ were used. These are approximations of the duration and velocity amplitude of the main pulse. Figure 1 indicates that a simple one-sine pulse can capture some of the kinematic characteristics of the motion recorded at the Lucerne Valley station. On the other hand, the resulting acceleration amplitude, $a_p = \omega_p v_p/2 = 0.045g$, is one order of magnitude smaller than the recorded peak ground acceleration.

Figure 2 (left) shows the acceleration, velocity and displacement histories of the fault-normal motions recorded at the El Centro Station Array #5 during the 15 October 1979 Imperial Valley

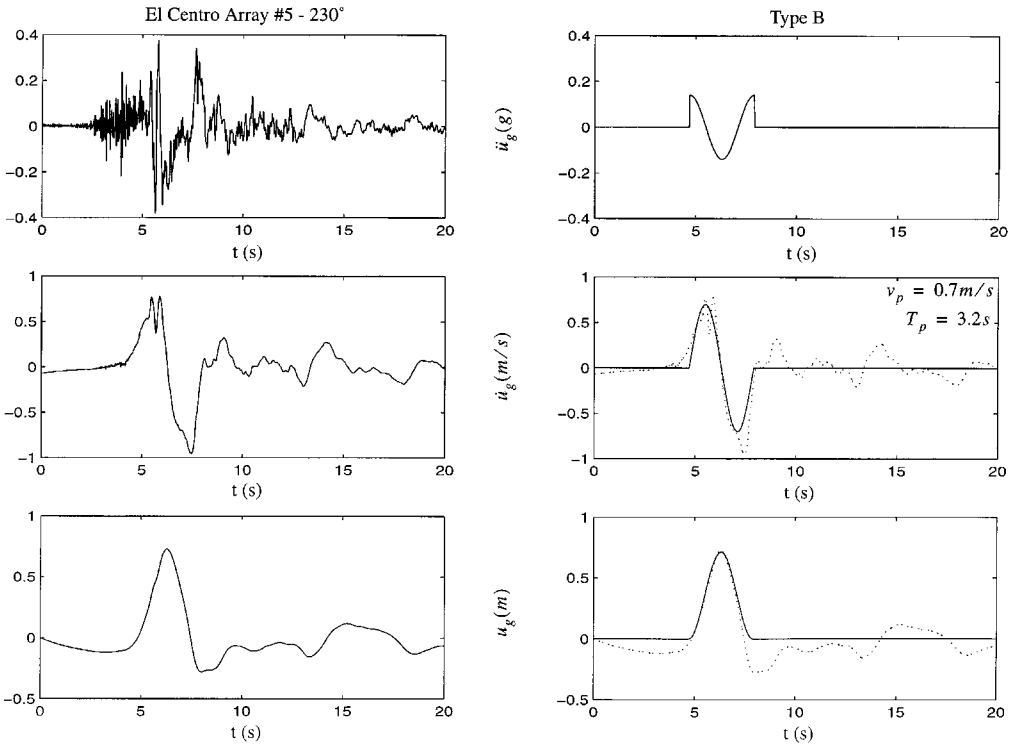

Figure 2. Fault parallel components of the acceleration, velocity and displacement time histories recorded at the El Centro Array #5 station during the 15 October 1979 Imperial Valley, California earthquake (left), and a cycloidal type-B pulse (right).

earthquake. This motion resulted in a forward-and-back pulse with a 3.2 sec duration. In this case, the coherent long period pulse is distinguishable not only in the displacement and velocity record, but also in the acceleration record. Figure 2 (right) plots the acceleration, velocity and displacement histories of a type-B cycloidal pulse given by Makris [10].

$$\ddot{u}_g(t) = \omega_p v_p \cos(\omega_p t), \quad 0 \leqslant t \leqslant T_p \tag{4}$$

$$\dot{u}_g(t) = v_p \sin(\omega_p t), \quad 0 \leqslant t \leqslant T_p \tag{5}$$

$$u_g(t) = \frac{v_p}{\omega_p} - \frac{v_p}{\omega_p} \cos(\omega_p t), \quad 0 \leqslant t \leqslant T_p \tag{6}$$

In constructing Figure 2 (right), the values $T_p = 3.2$ s and $v_p = 0.7$ m/s were used as approximate values of the pulse period and velocity amplitude of the recorded motions shown in Figure 2 (left).

Figure 3 (left) portrays the fault-normal components of the acceleration, velocity and displacement histories of the 17 January 1994 Northridge earthquake recorded at the Rinaldi station. This motion resulted in a forward ground displacement that recovered partially. The velocity history has a large positive pulse and a smaller negative pulse that is responsible for the partial

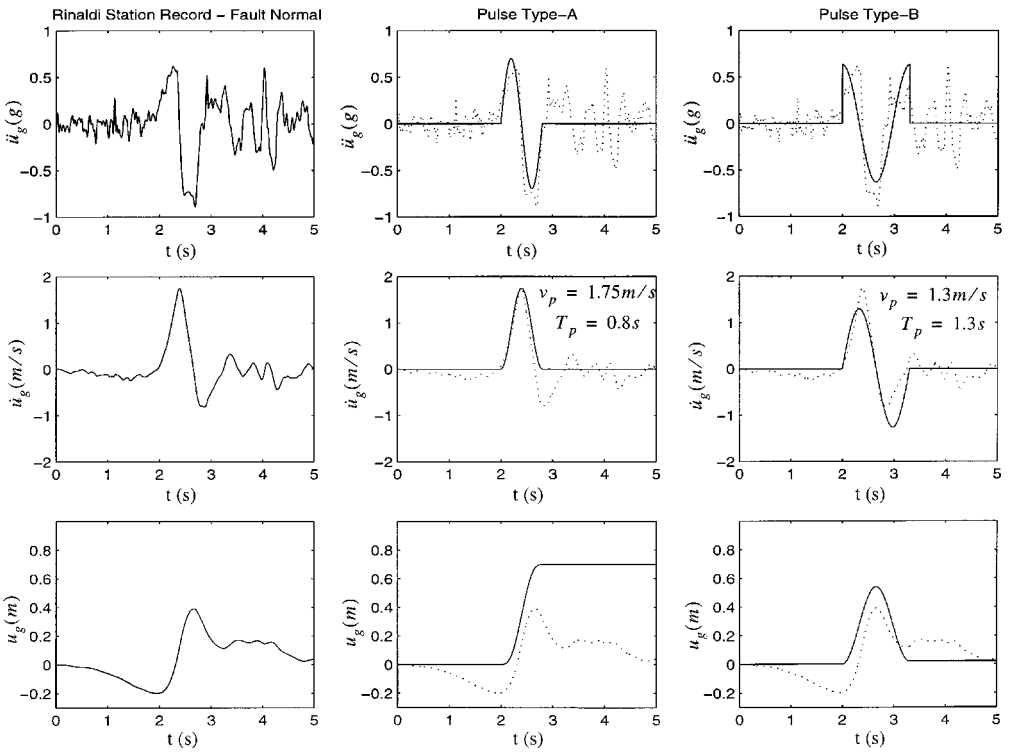

Figure 3. Fault normal components of the acceleration, velocity and displacement time histories recorded at the Rinaldi station during the 17 January 1994 Northridge, California earthquake (left), a cycloidal type-A pulse (center) and a cycloidal type-B (right).

recovery of the ground displacement. Accordingly, the fault normal component of the Rinaldi station record is in between a forward and a forward-and-back pulse. Figure 3 (centre) shows the results of Equations (1)–(3) by assuming a pulse duration $T_p = 0.8$ s and a velocity amplitude $v_p = 1.75$ m/s, which are approximations of the duration and velocity amplitude of the first main pulse shown in the record. Figure 3 (right) shows the results of Equation (4)–(6) by considering a pulse duration $T_p = 1.3$ sec and a velocity amplitude $v_p = 1.3$ m/s.

Not all near-source records are forward or forward-and-back pulses. Figure 4 (left) portrays the fault-normal component of the acceleration, velocity and displacement time histories recorded at the Sylmar station during the 17 January 1994 Northridge earthquake. The ground displacement consists of two main long period cycles, the first cycle being the largest, and the subsequent ones decaying. These long period pulses are also distinguishable in the ground velocity history where the amplitude of the positive pulses is larger than the amplitude of the negative pulses. Figure 5 (left) portrays the fault parallel components of the acceleration, velocity and displacement histories recorded at the Rinaldi station during the 17 January 1994 Northridge earthquake. The ground displacement consists of two main long-period cycles with subsequently decaying motions. Near-fault ground motions, where the displacement history exhibits one or more long duration cycles, are approximated with type-C pulses. An n-cycle ground displacement is

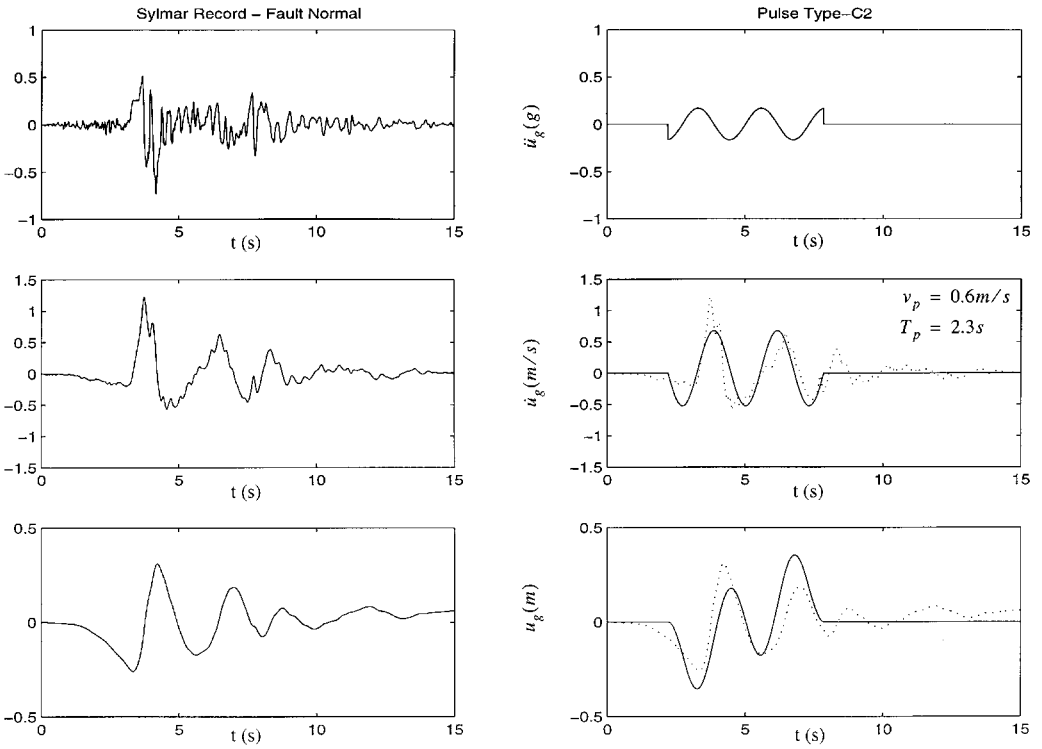

Figure 4. Fault normal components of the acceleration, velocity and displacement time histories recorded at the Sylmar station during the 17 January 1994 Northridge, California earthquake (left), and a cycloidal type-C_2 pulse (right).

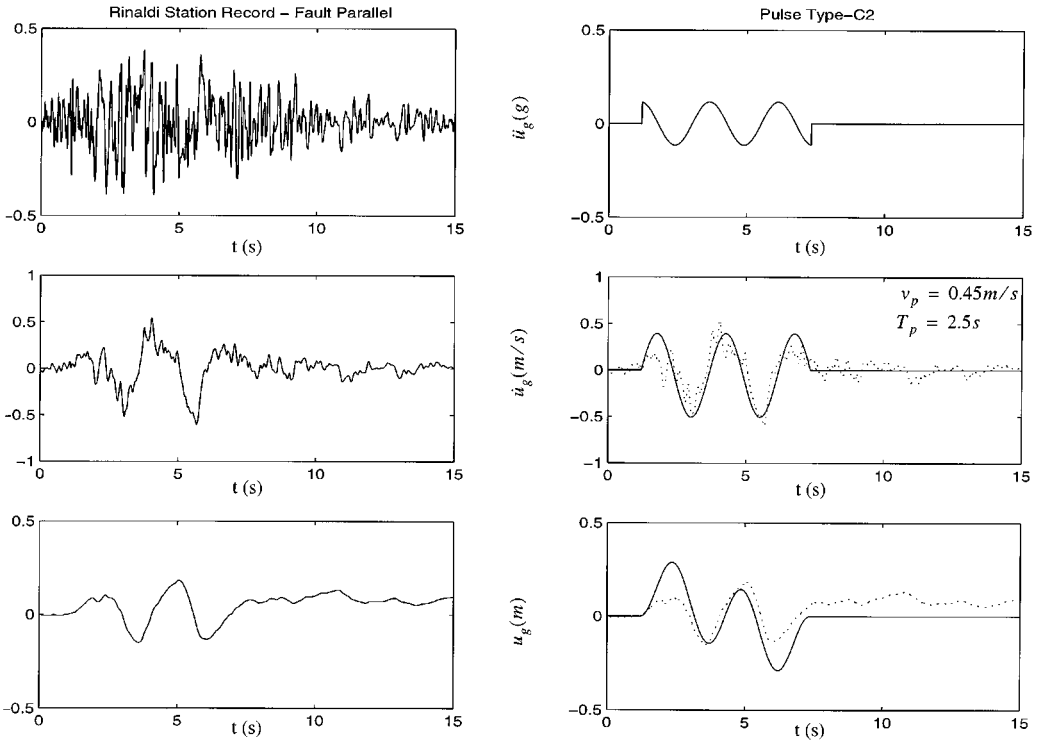

Figure 5. Fault parallel components of the acceleration, velocity and displacement time histories recorded at the Rinaldi station during the 17 January 1994 Northridge, California earthquake (left), a cycloidal type-C_2 pulse (right).

approximated with a type-C_n pulse, which is defined as

$$\ddot{u}_g(t) = \omega_p v_p \cos(\omega_p t + \varphi), \quad 0 \leqslant t \leqslant \left(n + \frac{1}{2} - \frac{\varphi}{\pi}\right) T_p \tag{7}$$

$$\dot{u}_g(t) = v_p \sin(\omega_p t + \varphi) - v_p \sin(\varphi), \quad 0 \leqslant t \leqslant \left(n + \frac{1}{2} - \frac{\varphi}{\pi}\right) T_p \tag{8}$$

$$u_g(t) = -\frac{v_p}{\omega_p} \cos(\omega_p t + \varphi) - v_p t \sin(\varphi) + \frac{v_p}{\omega_p} \cos(\varphi), \quad 0 \leqslant t \leqslant \left(n + \frac{1}{2} - \frac{\varphi}{\pi}\right) T_p \tag{9}$$

In deriving these expressions it is required that the displacement and velocity are differentiable signals. The value of the phase angle, φ, is determined by requiring that the ground displacement at the end of the pulse be zero. A type-C_n pulse with frequency $\omega_p = 2\pi/T_p$ has duration $T = (n + 1/2)\,T_p - 2\varphi/\omega_p = (n + 1/2 - \varphi/\pi)\,T_p$. In order to have a zero ground displacement at the end of type-C_n pulse

$$\int_0^{(n+1/2-\varphi/\pi)\,T_p} \dot{u}_g(t)\,\mathrm{d}t = 0 \tag{10}$$

Equation (10), after evaluating the integral, gives

$$\cos[(2n+1)\pi - \varphi] + [(2n+1)\pi - 2\varphi]\sin\varphi - \cos\varphi = 0 \tag{11}$$

The solution of the transcendental equation given by Equation (11) gives the value of the phase angle φ. For example, for a type-C_1 pulse ($n = 1$), $\varphi = 0.0697\pi$; whereas, for a type-C_1 pulse ($n = 2$), $\varphi = 0.0410\pi$.

MODELLING OF THE DISSIPATION MECHANISMS OF PRACTICAL ISOLATION SYSTEMS

In this study, we consider idealized isolated structures either with one or two degree of freedom. Figure 6 shows a schematic of these idealizations where the restoring force of the isolation system is assumed linear with stiffness K_I. For the 1-DOF idealization, $K_I = m\omega_I^2$. For the 2-DOF idealization, $K_I = (m_b + m)\omega_I^2$ where ω_I is the isolation frequency, m_b is the mass of the base and m is the mass of the superstructure. The natural frequency of the fixed base superstructure is $\omega_s = \sqrt{K_s/m}$. The damping of the superstructure is assumed equivalent viscous, satisfying the relation $C_s = 2\xi_s m\omega_s$. The damping of the isolation system is represented with various dissipation mechanisms which are approximated with idealized macroscopic models. Figure 7 shows the force–displacement loops of five dissipation mechanisms: (a) viscous model (high damping rubber bearings and viscous fluid dampers); (b) rigid–plastic model (sliding bearings); (c) elastic–plastic model (lead rubber bearings); (d) viscoplastic model (sliding bearings and viscous fluid dampers,

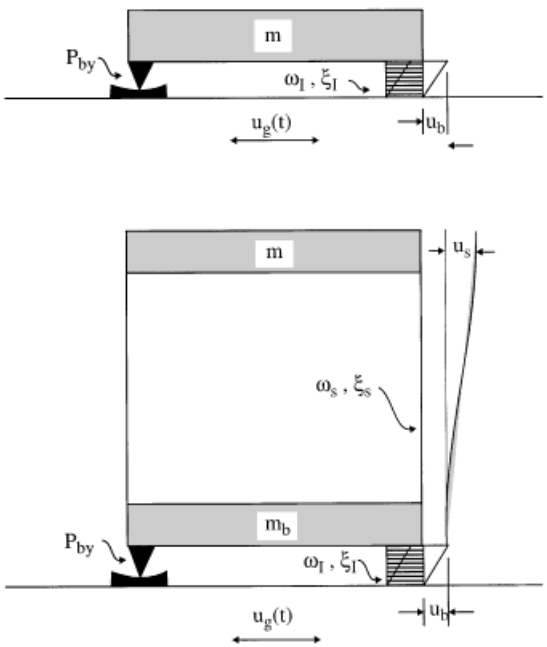

Figure 6. Schematic of an isolated rigid block (top) and of a 2-DOF isolated structure (bottom).

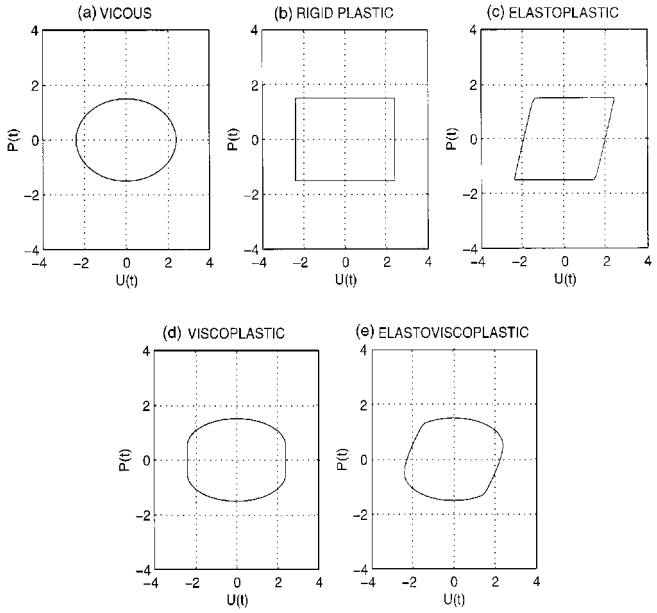

Figure 7. Five idealizations of energy dissipation mechanisms of practical seismic isolation systems.

elastometric bearings and friction dampers, elastometric bearings and controllable fluid dampers, sliding bearings and controllable fluid dampers); (e) elastoviscoplastic model (lead rubber bearings and viscous dampers).

It is worth mentioning that case 2 is the limiting case of 3, where the yield displacement becomes very small, whereas case 2 is also the limiting case of 4, where the viscous component vanishes. Accordingly, the dissipative behaviour of a sliding bearing is the limiting case of dissipative behaviour of a lead rubber bearing with a very small yield displacement. The elastoviscoplastic case 5 is the most general case, and the dissipation force can be expressed mathematically with

$$P(t) = C_1 \dot{u}_b(t) + K_1 u_y z(t) \tag{12}$$

where u_b is the base displacement shown in Figure 1 (bottom), K_1 is some reference stiffness, u_y is the value of the yield displacement of the isolation system and z is a hysteretic dimensionless quantity that is governed by the following equation:

$$u_y \dot{z} + \gamma |\dot{u}_b(t)| z |z|^{n-1} + \beta \dot{u}_b(t) |z|^n - A \dot{u}_b(t) = 0 \tag{13}$$

The model given by Equations (12) and (13) is a special case of the Bouc–Wen model [11, 12] enhanced with a viscous term. In equation (13), β, γ, n and A are dimensionless quantities that control the shape of the hysteretic loop. It can be shown that when $A = 1$, parameter K_1 in Equation (12) becomes the pre-yielding elastic stiffness. As an example, in a lead rubber bearing, K_1 is the stiffness of the lead core before yielding. Based on this observation, parameter A is set equal to one. C_I is the viscous damping coefficient of the isolation system $C_I = C_b + C_d$, where

$C_b = 2\xi_b(m + m_b)\omega_I$ is the viscous damping originating from the elastometric bearings, and $C_d = 2\xi_d(m + m_b)\omega_I$ is the viscous damping originating from possible additional damping devices.

For the special case of rigid viscoplastic behaviour, the yield displacement $u_y \to 0$ and the pre-yielding stiffness $K_e \to \infty$ so that the product $u_y K_e \to P_y$, which is the finite yield force. Under these conditions, Equation (12) reduces to the Bingham model of viscoplasticity [13],

$$P(t) = C_I \dot{u}_b(t) + P_y \operatorname{sgn}[\dot{u}_b(t)] \tag{14}$$

in which $P_y = P_{by} + P_{dy}$, where $P_{by} = \mu(m + m_b)g$ is the yield (friction type) force originating from the sliding bearing, and P_{dy} is the yield force that might originate from additional damping devices such as controllable fluid dampers. When sliding teflon bearings are used, the pre-yield stiffness is large but finite. Accordingly, even for sliding teflon bearings, the behaviour is elasto-plastic with a small yield displacement [14] ($u_y = 0.2$ mm). For, lead-rubber bearing, the elastoplastic model is also appropriate; however, the yield displacement is of the order of centimeters. With reference to Figure 1(a), the equation of motion of the 1-DOF system is

$$\ddot{u}_b(t) + \alpha(t) + \omega_b^2 u(t) = -\ddot{u}_g(t) \tag{15}$$

and with reference to Figure 1(b), the equation of motion of the 2-DOF system is expresses as follows [15]:

$$\begin{bmatrix} 1 & \gamma_m \\ 1 & 1 \end{bmatrix} \begin{bmatrix} \ddot{u}_b(t) \\ \ddot{u}_s(t) \end{bmatrix} + \begin{bmatrix} 0 & 0 \\ 0 & 2\xi_s\omega_s \end{bmatrix} \begin{bmatrix} \dot{u}_b(t) \\ \dot{u}_s(t) \end{bmatrix} + \begin{bmatrix} \omega_b^2 & 0 \\ 0 & \omega_s^2 \end{bmatrix} \begin{bmatrix} u_b(t) \\ u_s(t) \end{bmatrix} + \begin{bmatrix} 1 \\ 0 \end{bmatrix} \alpha(t) = -\begin{bmatrix} 1 \\ 1 \end{bmatrix} \ddot{u}_g(t) \tag{16}$$

where $\gamma_m = m_s/(m + m_b)$ and $\alpha(t) = P(t)/(m + m_b)$, in which $P(t)$ is the dissipation force given by Equations (12) or (14). The parametric analysis presented in this paper is conducted by solving Equations (15) and (16) for various representations of the dissipative force $P(t)$. The response of the 2-DOF structure shown in Figure 1 (bottom), which is expressed with Equation (16), is computed using a state-space formulation where the state vector of the system is $y(t) = \langle u_b(t), \dot{u}_b(t), u_s(t), \dot{u}_s(t), z(t) \rangle^T$.

PARAMETRIC STUDY

The formulation presented in the previous section can provide valuable information on the one-dimensional response of isolated freeway overcrossings. Some of the recently constructed freeway overcrossings in California are either isolated at the end-abutments and centre bent, or are supported on isolators at the end-abutments while they are rigidly connected at the centre bent. This later configuration results to 'isolation' periods $T_I = 1$ sec or even less [16].

The scope of this parametric study is to provide information on the efficiency of various combinations of dissipation mechanism to suppress the earthquake response. First, various levels of viscous damping alone are considered. Subsequently, various levels of friction (plastic) forces are considered where: (a) the yield displacement is very small ($u_y = 0.2$ mm) and; (b) the yield displacement is finite ($u_y = 10$ and 20 mm) . This distinction is done in order to observe potential differences between a 'rigid' plastic and an elastic plastic model that will reflect the behaviour of a teflon sliding bearing and a lead rubber bearing, respectively, with the same yield force. When

viscous damping alone is considered, the levels of viscous damping in the isolation system have been chosen to be $\xi_I = 5$, 15 and 30 per cent. Isolation systems with $\xi_I = 15$ per cent are common; whereas, $\xi_I = 30$ per cent is at the high end. The levels of the coefficient of friction selected in this study are $\mu = 6$, 9 and 18 per cent. Values of $\mu = 6$ and 9 per cent are typical values of friction coefficients on commercially available sliding bearings. The value of $\mu = 18$ per cent was selected to illustrate the effects of high-value of dry friction.

The first column in Figure 8 shows the response of a 1-DOF overcrossing with isolation period $T_I = 2$ sec and viscous isolation damping $\xi_I = 15$ per cent subjected to the type-A cycloidal front with $T_p = 1.0$ sec and the Rinaldi station record shown in Figure 3. For the type-A pulse (first and second row), relative displacements reach 50 cm (20 in); whereas the base shear coefficient exceeds the value of 0.5. The second column in Figure 8 plots the response of the isolated structure where the isolation damping has been doubled by adding viscous dampers, $\xi_I = \xi_b + \xi_d = 30$ per cent. With a total isolation damping coefficient of $\xi_I = 30$ per cent, the base displacement reduces by 30 per cent (35 cm) and the base shear reduces by 15 per cent. The reason that the base shear reduces under the presence of twice the viscous damping is because, although

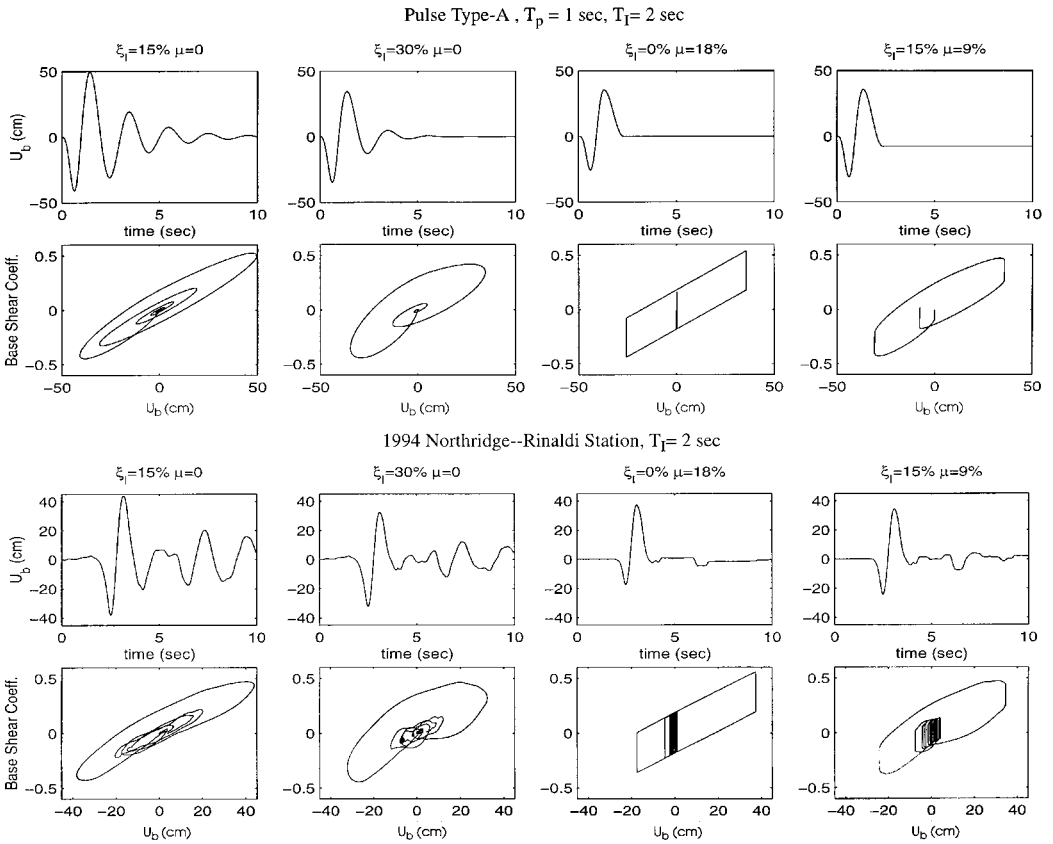

Figure 8. Response quantities of an isolated block with $T_I = 2$ sec subjected to a type-A pulse with $T_p = 1$ sec (top) and to the Rinaldi station record (bottom).

additional damping increases the damping forces, it decreases displacements, resulting in smaller elastic forces.

The third column in Figure 8 plots the response of the isolated structure where the isolation damping is only of the friction type (rigid–plastic damping). It is shown that, for this system, ($T_I = 2$ sec); a coefficient of friction $\mu = 18$ per cent is needed to achieve the same displacement reduction that a 30 per cent viscous coefficient achieves. The last column in Figure 8 plots the response of the isolated structure that combines viscous damping, $\xi_I = 15$ per cent, and friction damping that corresponds to $\mu = 9$ per cent. This combination of viscous and friction damping achieves the same displacement reduction that was achieved with the two other configurations.

Figure 8 (bottom) shows the response of the same 1-DOF system with $T_1 = 2$ sec when excited by the Rinaldi station record. With viscous isolation damping $\xi_I = 15$ per cent, the maximum displacement is 44 cm which is 17 per cent less than the maximum displacement reached under a type-A pulse front with nearly the same velocity pulse. The increase of the isolation damping from $\xi_I = 15$ to 30 per cent reduced the response from 44 to 32.4 cm—a 30 per cent reduction, which is the same amount of reduction that is achieved in the case of a pulse type-A motion.

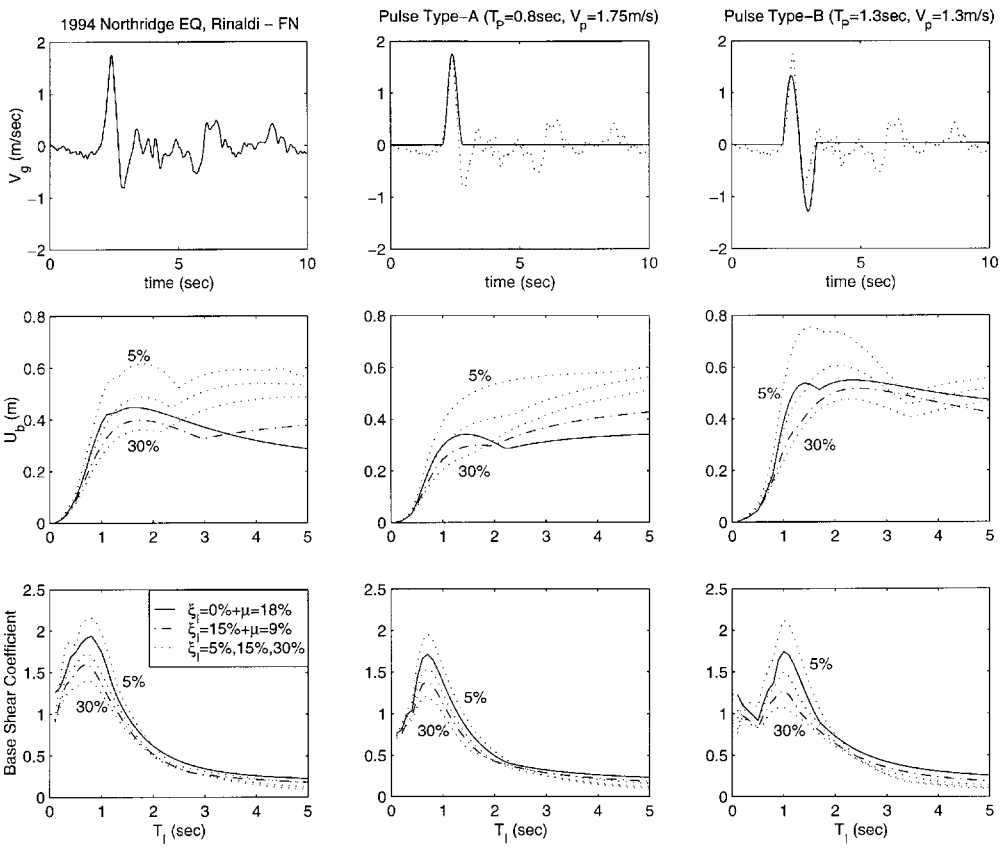

Figure 9. Displacement and base shear spectra of an isolated block subjected to the fault normal component of the Rinaldi station record (left), a type-A pulse (centre) and a type-B pulse (right).

The third column in Figure 8 plots the response of the 1-DOF system under rigid-plastic dissipation ($\mu = 18$ per cent). It is interesting to note that the maximum displacement is 37.4 cm, which is more than the displacement that was reached under a type-A pulse motion (see first row in Figure 8). Furthermore, the value of $\mu = 18$ per cent now results in a 5 cm larger displacement response than the response obtained with $\xi_I = 30$ per cent, and a 20 per cent larger base shear. Consequently, this example shows that two systems which are equivalent under one input exhibit opposite trends under a different but similar input.

The seismic performance of the rigid block equipped with various types of damping mechanisms in its isolation system is summarized in Figure 9, where displacement and base shear spectra are plotted for the fault normal component of the Rinaldi station record (left), a type-A pulse excitation with $T_p^A = 0.8$ sec (centre) and a type-B pulse excitation with $T_p^B = 1.3$ sec (right), and kinematic characteristics that approximate those of the Rinaldi station record. It is observed that, at the low isolation period range (i.e. $T_I < 2.0$ sec), additional viscous damping reduces the displacements and base shear in the most effective way. Friction dissipation alone ($\xi_I = 0$, $\mu = 18$ per cent) becomes effective in reducing displacement at large isolation periods, however, the

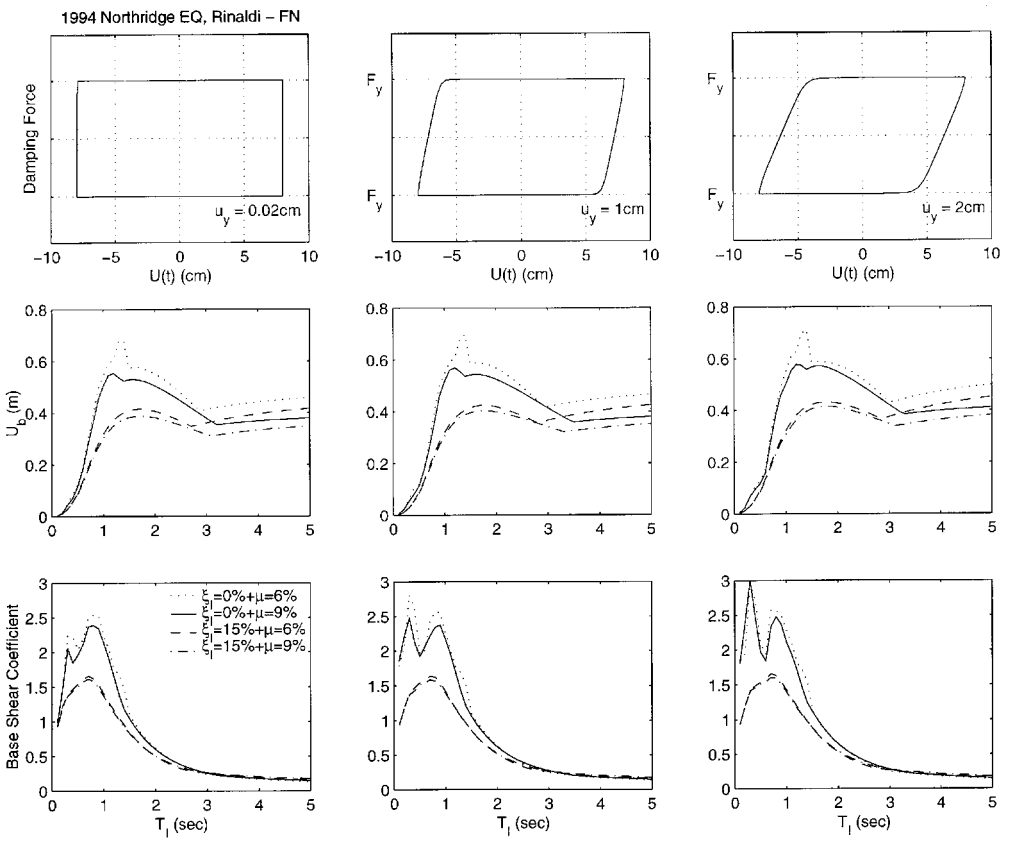

Figure 10. Displacement and base shear spectra of an isolated block subjected to the fault normal component of the Rinaldi station record. Left: $u_y = 0.2$ mm, centre $u_y = 10$ mm, right: $u_y = 20$ mm.

resulting base shear is the largest. A combination of viscous and friction damping results in an attractive performance, since the effective reduction of displacements is accompanied by base shear lower than that resulting from friction dissipation alone. For example, Figure 9 (left) indicates that an isolation period $T_I = 3.0$ sec with $\xi_I = 15$ per cent and $\mu = 9$ per cent will result to a base displacement of $u_b = 33$ cm and a base shear coefficient of 0.25. On the other hand, additional energy dissipation devices that will increase the damping of a 1 sec period structure from 5 to 30 per cent will reduce displacement to half; whereas the base shear will exceed the weight of the structure. Another interesting observation is that the response spectra of the fault normal component of the Rinaldi station record has a smooth shape, resembling the shape of the spectra obtained with the pulse type-A and pulse type-B excitations.

Figure 10 plots the displacement and base shear spectra of the fault normal component of the Rinaldi station and for three different values of yield displacements (left: $u_y = 0.2$ mm, centre: $u_y = 10$ mm, right: $u_y = 20$ mm). Two values of the yield force, $F_y = \mu W$, (W is the above-the-isolation system mass) have been selected ($\mu = 6$ and 9 per cent). Figure 10 shows that the

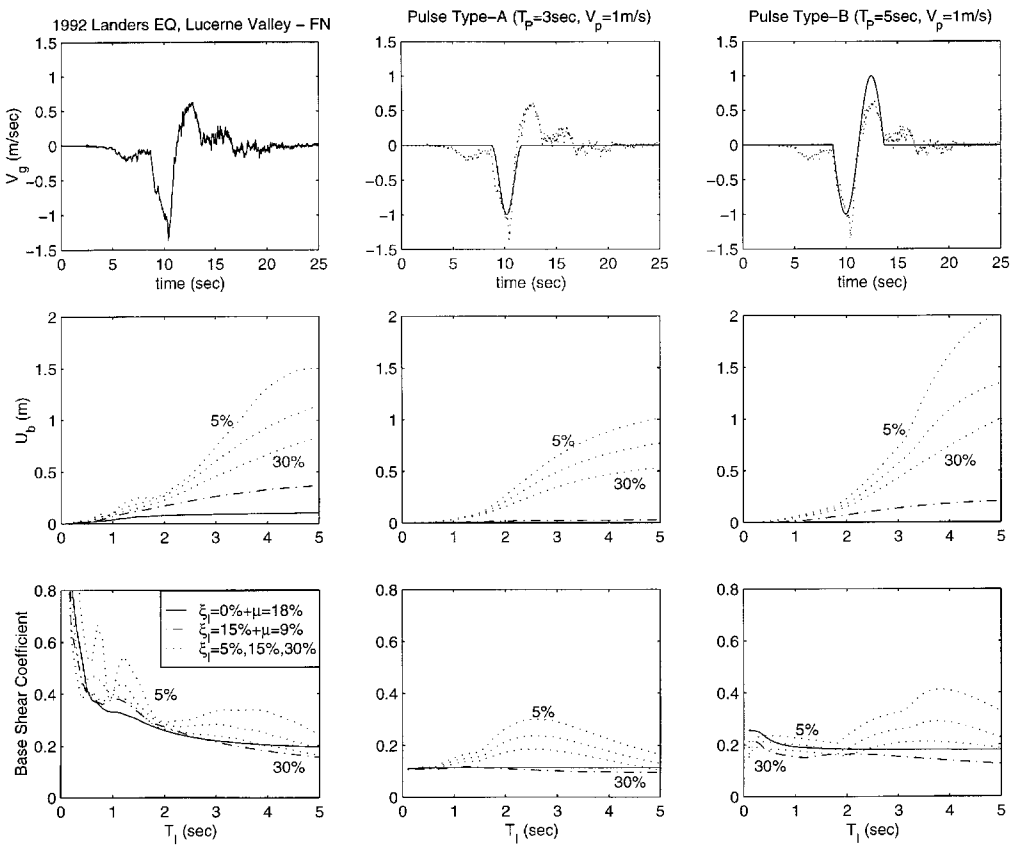

Figure 11. Displacement and base shear spectra of an isolated block subjected to the fault normal component of Lucerne Valley record (left), a type-A pulse (centre) and a type-B pulse (right).

value of the yield displacement has insignificant effect on the values of base displacements and base shears. Accordingly, rigid–plastic behaviour (sliding bearings) results to nearly the same response reduction as elastic–plastic behaviour (lead rubber bearings) provided that both systems have the same yield force, $F_y = \mu W$. In the absence of viscous dissipation ($\xi_I = 0$), an increment of the plastic (yield) force from 6 to 9 per cent suppress further resonant effects. However, under the presence of viscous force ($\xi_I = 15$ per cent), the increase of the plastic force from 6 to 9 per cent has a minor effect in both base displacements and base shears.

Figure 11 plots the displacement and base shear spectra of the fault normal component of the Lucerne Valley record (left), a type-A pulse with $T_p^A = 3$ sec (centre) and a type-B pulse with $T_p^B = 5$ sec (right) . In this case, friction dissipation alone results in the smallest displacement values; whereas, the combination of viscous and friction damping results in the smallest base shear values. In the low range of isolation periods ($T_I < 2.0$ sec), the spectrum from the recorded motion is substantially different from the spectrum that results from the pulse motions, indicating that, in the low isolation period range the response is governed by the high-frequency fluctuations

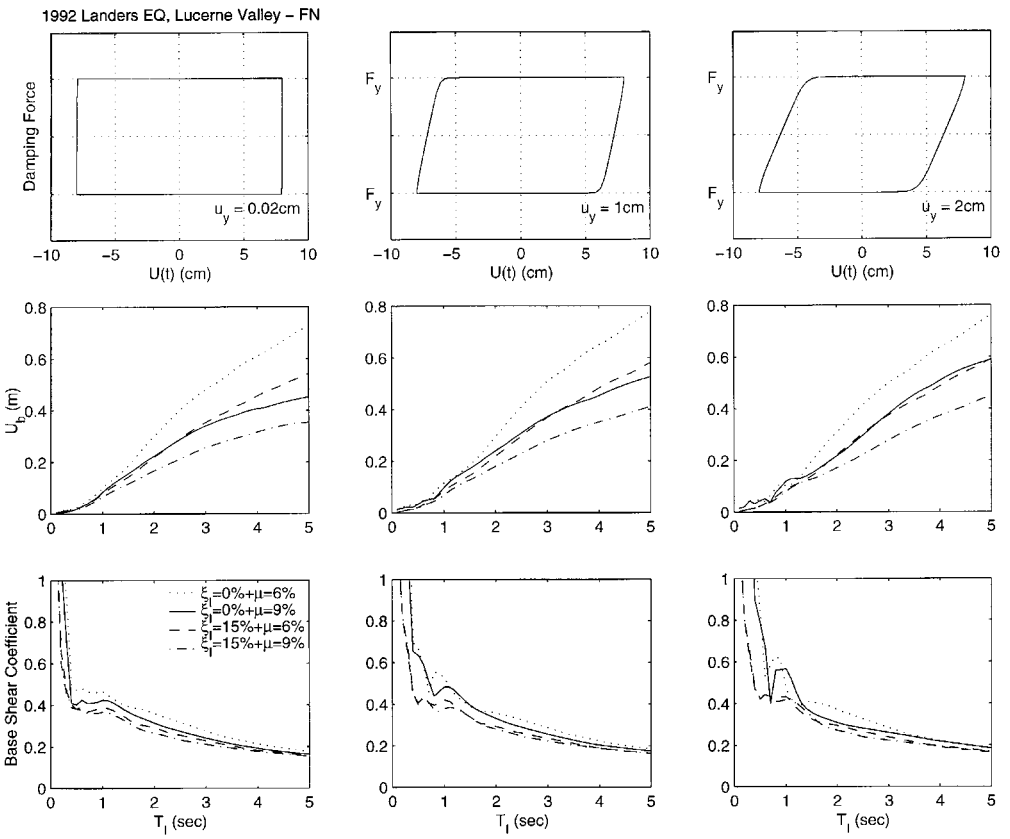

Figure 12. Displacement and base shear spectra of an isolated block subjected to the fault normal component of Lucerne Valley record. Left: $u_y = 0.2$ mm, centre $u_y = 10$ mm, right: $u_y = 20$ mm.

that override the long duration pulse. At the high range of isolated period ($T_I > 2.0$ sec), viscous dissipation results in large displacements that are substantially reduced when some friction dissipation is introduced. Again, a 3 sec isolation period with $\xi_I = 15$ per cent and $\mu = 9$ per cent results in an attractive design. Figure 12 shows the same response quantities for three different values of yield displacements ($u_y = 0.2$, 10 and 20 mm). Again, rigid–plastic behaviour (sliding bearings) results to nearly the same response reduction as elastic–plastic behaviour (lead rubber bearings). It is observed that in this case, the increase of plastic forces from $\mu = 6$ to 9 per cent has a noticeable effect under the absence and presence of viscous forces. Figure 12 also indicates that pure friction damping with $\mu = 9$ per cent has the same effect as viscoplastic damping with $\mu = 6$ per cent and $\xi_I = 15$ per cent.

Figure 13 plots the displacement and base shear spectra of the fault normal component of the El Centro Array #5 record (left) and a type-B pulse with $T_p^B = 3.2$ sec (right). In this case, viscous dissipation results not only in large displacement, but also in substantial base shear. Friction dissipation eliminates amplification due to resonance for isolation periods longer than 2 sec. A 3 sec isolation period with $\xi_I = 15$ per cent and $\mu = 9$ per cent again results in an attractive

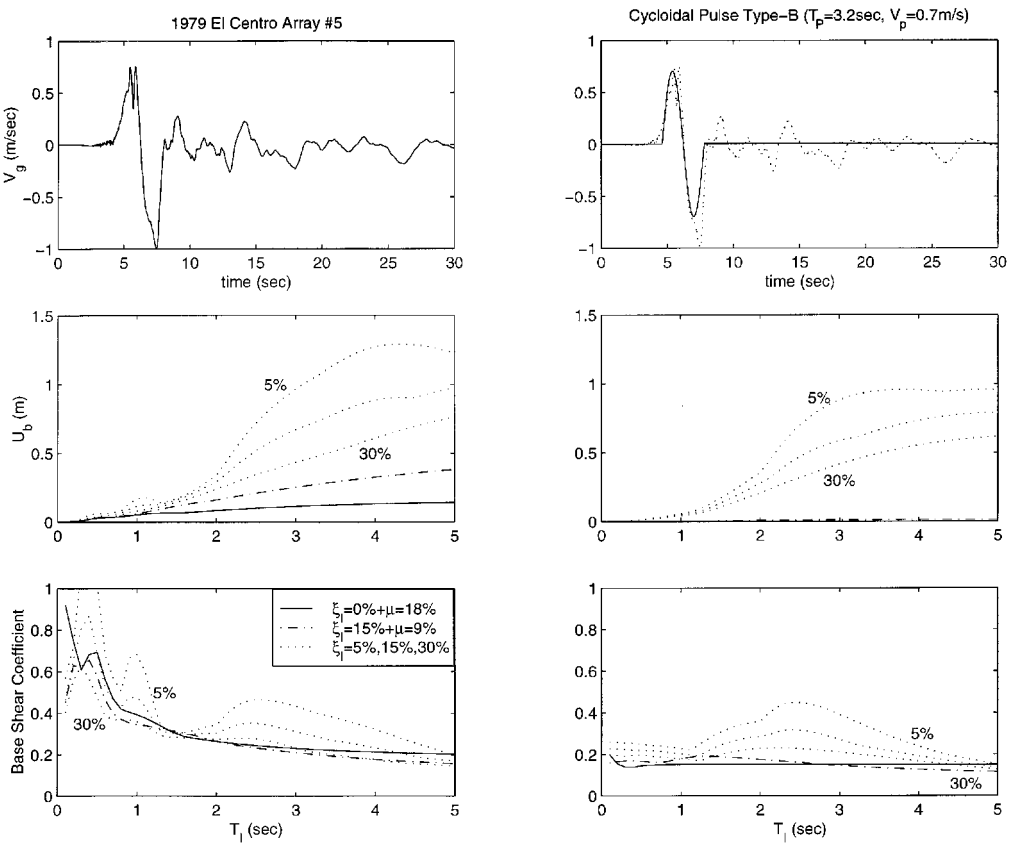

Figure 13. Displacement and base shear spectra of an isolated block subjected to the El Centro Array #5 station record (left) and a type-B pulse (right).

response, showing that there is no need for an extremely long isolation period (i.e., $T_I = 5$ sec) to protect structures from near-source ground motions. Figure 14 shows similar trends to those observed in Figure 12.

Figure 15 plots the displacement and base shear spectra of the fault normal component of the Sylmar record (left) and a type-C_2 pulse with $T_p^{C_2} = 2.3$ sec (right). The sensitivity of the response on the level of yield displacement is shown on Figure 16. Trends similar to those detected in Figure 10 are observed in this case. In the absence of viscous dissipation ($\xi_I = 0$), an increment of the plastic (yield) force from 6 to 9 per cent suppresses further resonant effects; however, under the presence of viscous force $\xi_I = 15$ per cent), the increment of the plastic (yield) force from 6 to 9 per cent has a less drastic effect.

This parametric study on the response of 1-DOF systems indicates that, under near-source ground motion plastic dissipation forces of the order of 9 per cent of the weight of the structure are very beneficial in reducing displacements without increasing base shears. Displacements can be further reduced with additional viscous damping. Furthermore, the ability to control the level of friction forces increases the effectiveness of the isolation system under certain motions.

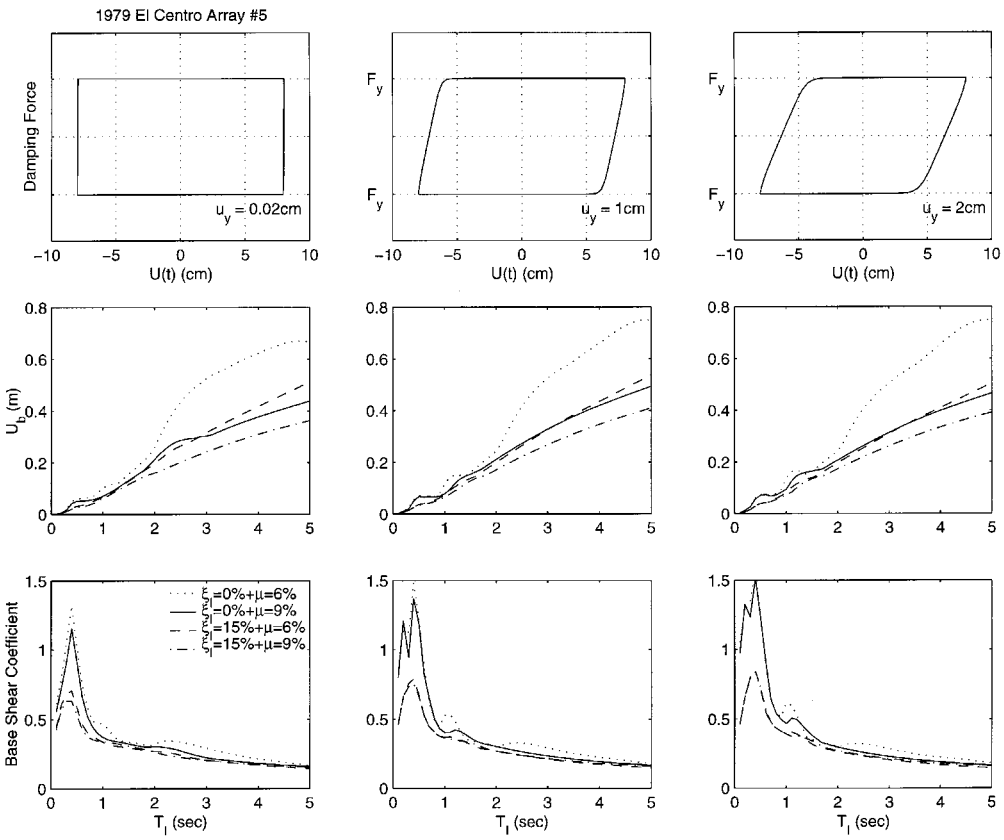

Figure 14. Displacement and base shear spectra of an isolated block subjected to the El Centro Array #5 station record. Left: $u_y = 0.2$ mm, centre $u_y = 10$ mm, right: $u_y = 20$ mm.

Accordingly, the findings of this study indicate the potential advantages that controllable fluid dampers have on seismic protection application [10].

We now investigate the effect of the viscous, viscoplastic and rigid-plastic dissipation mechanisms on the response of the 2-DOF structure shown in Figure 6 (bottom). As an example, Figure 17 plots the base displacement, base shear, superstructure drift and total acceleration time histories of the superstructure of a 2-DOF system equipped with the dissipation mechanisms introduced in the previous section. The isolation period is $T_I = 2.0$ sec, and the superstructure period is $T_I = 0.25$ sec. The response of the base of the 2-DOF structure when subjected to the Rinaldi station record is very close to the response of 1-DOF structure with the same isolation period ($T_I = 2$ sec) shown in Figure 8 (bottom). It is interesting to note that, by increasing the viscous damping from 15 to 30 per cent, the base displacement decreased from 43.7 to 32.2 cm (30 per cent), whereas the increase of interstorey drift was less 1 per cent and the increase in the superstructure acceleration was less than 2 per cent, which shows that, in this case, additional damping substantially decreased the base displacement without affecting interstorey drifts and superstructure accelerations. However, when friction damping is used ($\mu = 18$ per cent), the

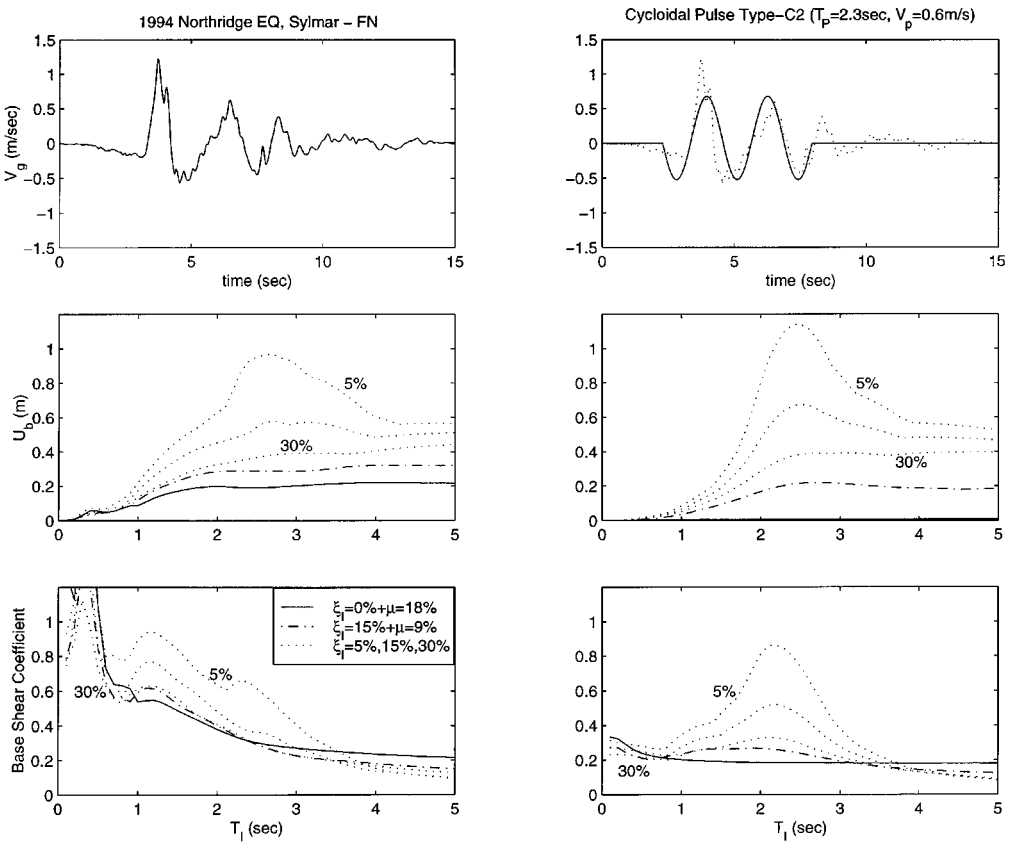

Figure 15. Displacement and base shear spectra of an isolated block subjected to the Sylmar station record (left) and a type-C_2 pulse (right).

displacements are reduced only to 37.3 cm (16 per cent), whereas interstorey drift is increased by 45 per cent, and superstructure acceleration is also increased by 45 per cent. The combination of viscous ($\xi_I = 15$ per cent) and hysteretic ($\mu = 9$ per cent) dissipation reduced base displacements to 34.6 cm (23 per cent reduction), whereas interstorey drift increased by 27 per cent and sùperstructure acceleration increased by 30 per cent.

The seismic performance of the 2-DOF isolated structure equipped with various types of damping mechanisms in its isolation system is summarized in Figure 18, where displacement, base shear, interstorey drift and superstructure acceleration spectra are plotted for the fault normal component of the Rinaldi station record (left), a type-A pulse excitation with $T_p^A = 0.8$ sec (center) and a type-B pulse excitation with $T_p^B = 1.3$ sec (right). In this case, supplemental energy dissipation with viscous damping outperforms all other dissipation mechanisms. In contrast, Figure 19 shows that, under the Sylmar motion of the 1994 Northridge earthquake, an isolation system with $T_I = 3$ sec and a combination of viscous damping $\xi_I = 15$ per cent and friction damping $\mu = 9$ per cent results in the most attractive response.

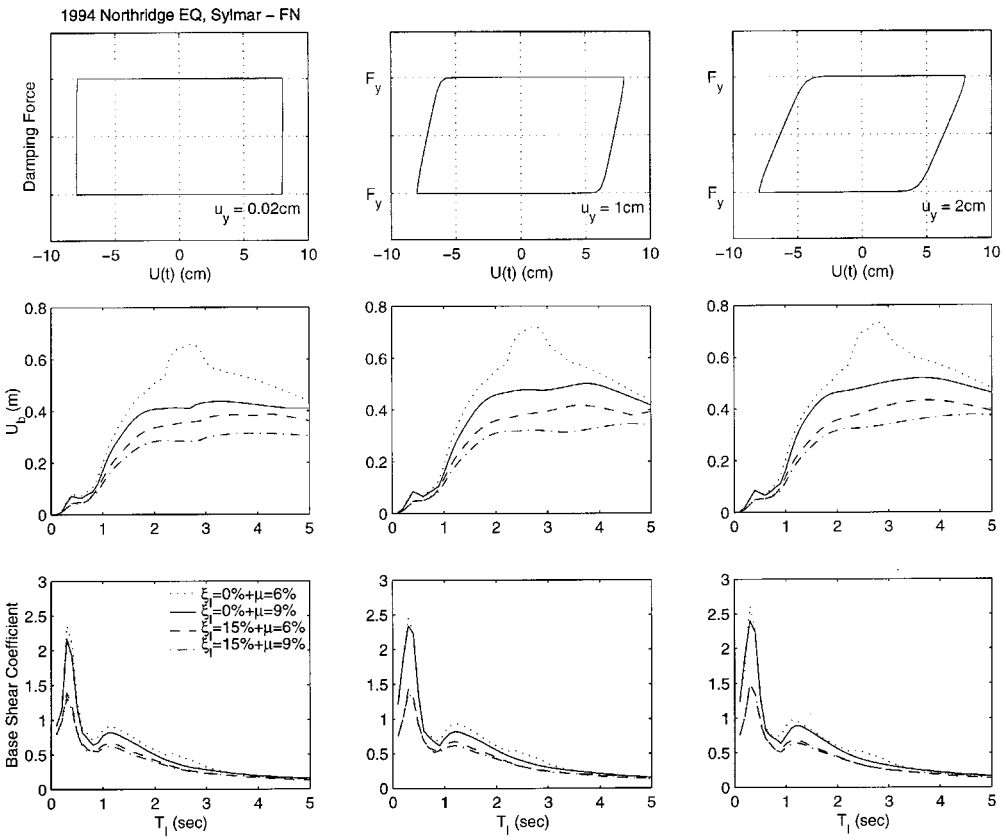

Figure 16. Displacement and base shear spectra of an isolated block subjected to the Sylmar station record. Left: $u_y = 0.2$ mm, centre $u_y = 10$ mm, right: $u_y = 20$ mm.

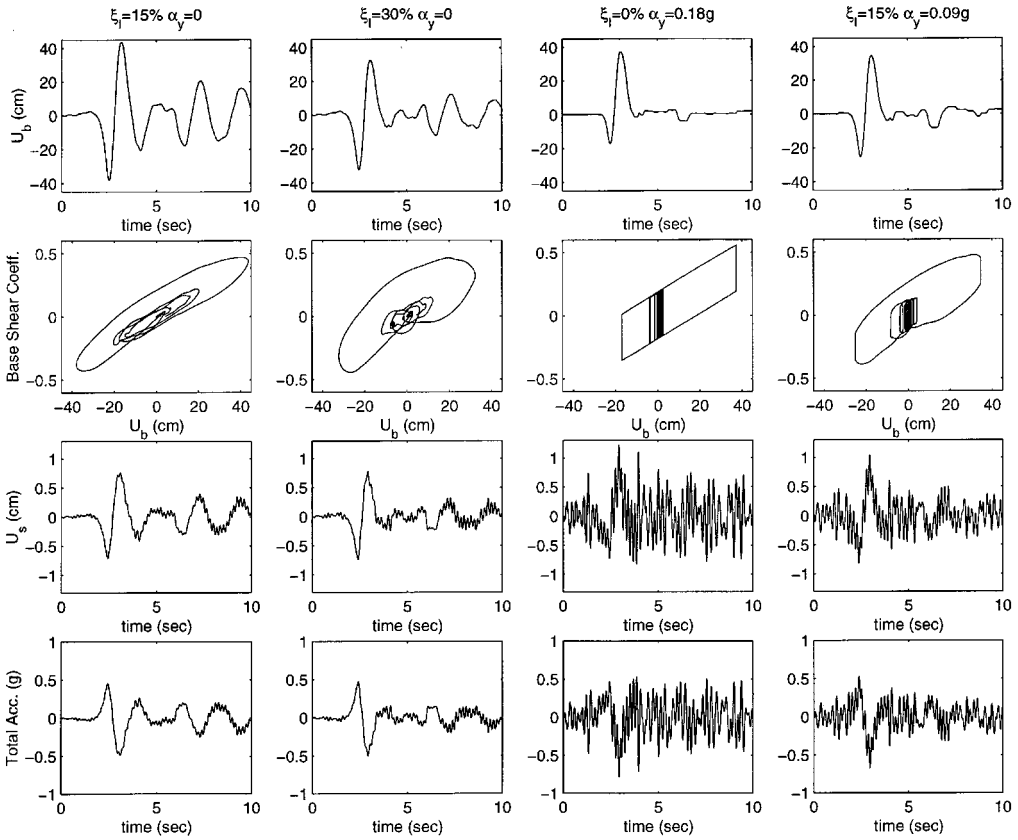

Figure 17. Response quantities of a 2-DOF isolated structure subjected to the fault normal component of the Rinaldi station record.

CONCLUSIONS

The efficiency of various dissipative mechanisms to protect isolated structures from pulse-type near-source ground motion has been investigated in detail. Physically realizable trigonometric pulses have been introduced, and their resemblance to selected near-source ground motions was illustrated. It is found that structural response quantities due to the recorded motions resemble the structural response quantities due to trigonometric pulse-type motions only when the isolation period reaches high values (i.e., $T_I = 3.0$ sec or more). The response of structures with relatively low isolation periods (i.e., $T_I < 2.0$ sec) is substantially affected by the high frequency that overrides the long-duration pulse. Therefore, the concept of seismic isolation is beneficial even for motions that contain long-velocity and displacement pulses. It is observed that a relatively low value of plastic (friction) damping (i.e. $\mu = 9$ per cent) removes any resonant effect that a long-duration pulse has a long-period isolation system. According to this study, there is no need for extremely long isolation periods (i.e. $T_I = 5.0$) in order to go further away from the long period pulse that dominates a near-source ground motion. The study shows that the benefits of

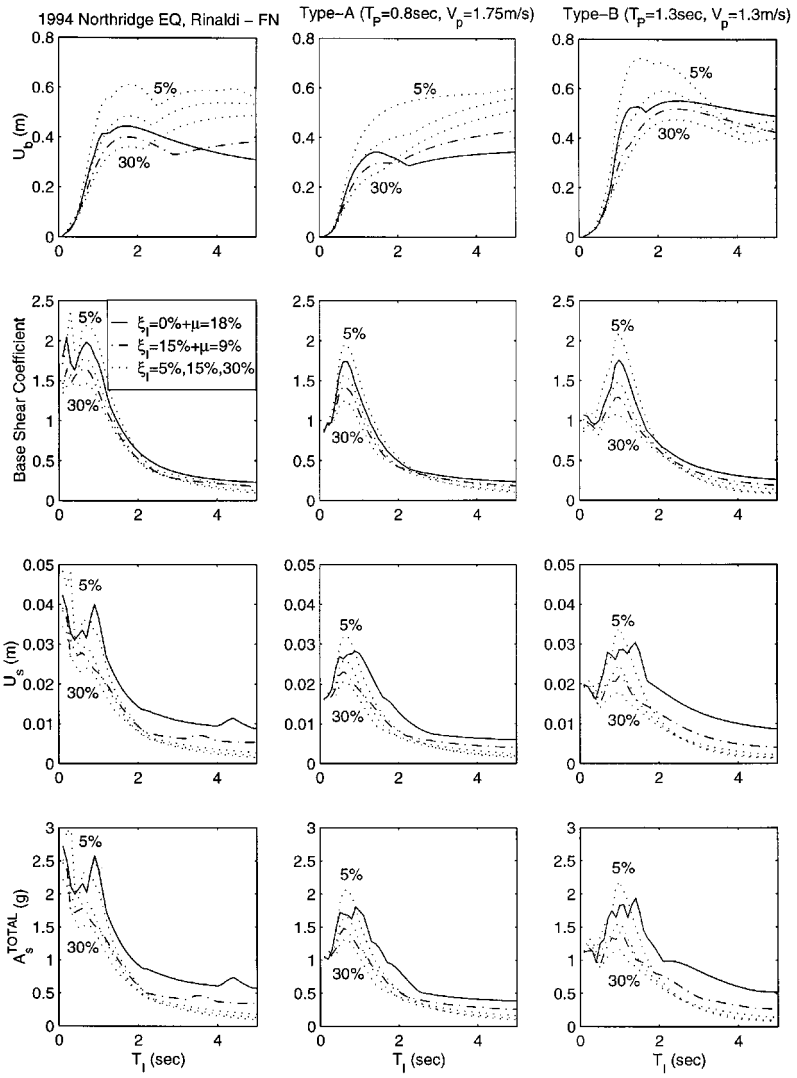

Figure 18. Base displacement, base shear, superstructure drift and total superstructure acceleration spectra of a 2-DOF isolated structure subjected to the fault normal component of the Rinaldi station record (left), a type-A pulse (centre) and a type-B pulse (right).

hysteretic dissipation are nearly indifferent to the level of the yield displacement and that they depend primarily on the level of the plastic (friction) force. Consequently, rigid–plastic behaviour (sliding bearings) results to nearly the same response reduction as elastic–plastic behaviour (lead rubber bearings) provided that both systems have the same yield (friction) force. The study concludes that, for isolated structures with isolation period $T_I = 3.0$ sec, a combination of viscous and friction dissipation forces is attractive, since displacements are substantially reduced without appreciably increasing base shears and superstructure accelerations. The study makes clear that

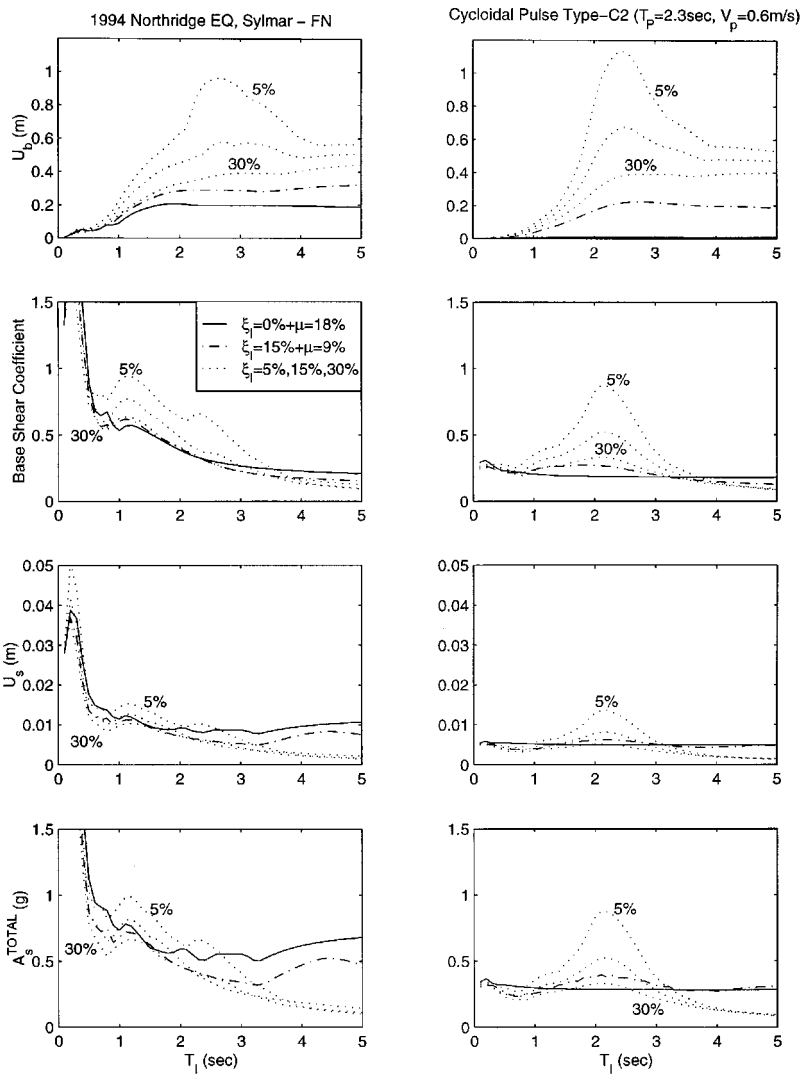

Figure 19. Base displacement, base shear, superstructure drift and total superstructure acceleration spectra of a 2-DOF isolated structure subjected to the fault normal component of the Sylmar station record (left), a type-C_2 pulse (right).

under near-source ground motion, a time domain dynamic analysis is needed where the mechanical properties of isolation system are accounted for.

ACKNOWLEDGEMENTS

Partial financial support for this study was provided by the National Science Foundation under Grant CMS-9696241 and the California Department of Transportation under Grant RTA-59A169.

REFERENCES

1. ATC-17-1. *Proceedings of Seminar on Seismic Isolation, Passive Energy Dissipation and Active Control*, vol. 1&2, Applied Technology Council, 1993.
2. Inaudi JA, Kelly JM. Optimum damping in linear isolation systems. *Earthquake Engineering and Structural Dynamics* 1993; **22**:583–598.
3. Anderson JG, Bodin P, Brune JN, Prince J, Sing SK. Strong ground motion from the Michoagan, Mexico earthquake. *Science*, 1986; **233**:1043–1049.
4. Campillo M, Gariel JC, Aki K, Sanchez-Sesma FJ. Destructive strong ground motions in Mexico City: Source, path, and site effects during great 1985 Michoagan earthquake. *Bulletin Seismological Society of America* 1989; **79**:1718–1735.
5. Iwan WD, Chen XD. Important near-field ground motion data from the Landers earthquake. *Proceedings of the 10th European Conference on Earthquake Engineering*. Balkema: Rotterdam, 1994.
6. Anderson JC, Bertero V. Uncertainties in establishing design earthquakes. ASCE *Journal of Structural Engineering* 1986; **113**:1705–1724.
7. Hall JF, Heaton TH, Halling MW, Wald DJ. Near-source ground motions and its effects on flexible buildings. *Earthquake Spectra* 1995; **11**:569–605.
8. Iwan WD. Drift spectrum: measure of demand for earthquake ground motions. *Journal of Structural Engineering* 1997; **123**:397–404.
9. Jacobsen LS, Ayre RS. *Engineering Vibrations*. McGraw-Hill: New York, 1958.
10. Makris N. Rigidity–plasticity–viscosity: can electrorheological dampers protect base-isolated structures from near-source ground motions? *Earthquake Engineering and Structural Dynamics* 1997; **26**:571–591.
11. Wen YK. Approximate method for nonlinear random vibration. ASCE *Journal of the Engineering Mechanics Division* 1975; **101**:389–401.
12. Wen YK. Method for random vibration of hysteretic systems, ASCE *Journal of the Engineering Mechanics Division* 1976; **102**:249–263.
13. Shames IH, Cozzarelli FA. *Elastic and Inelastic Stress Analysis*. Prentice-Hall: Englewood Cliffs, NJ, 1992.
14. Mokha A, Constantinou MC, Reinhorn AM. Teflon bearings in aseismic base isolation: experimental studies and mathematical modelling. *Technical Report NCEER-88-0038*, SUNY-Buffalo, NY, 1988.
15. Kelly JM. *Earthquake Resistant Design with Rubber*. Springer: London, 1997.
16. Delis E, Tokas C, Madani M, Thompson KJ. Analytical studies for seismic isolation in highway bridges. *Structures Congress* XV 1997; **2**:1471–1478.

